PHYSICAL REVIEW D **85,** 094513 (2012)

Modeling the gluon propagator in Landau gauge: Lattice estimates of pole masses and dimension-two condensates

A. Cucchieri,[1,2,*] D. Dudal,[1,†] T. Mendes,[2,‡] and N. Vandersickel[1,§]

[1]*Ghent University, Department of Physics and Astronomy, Krijgslaan 281-S9, 9000 Gent, Belgium*
[2]*Instituto de Física de São Carlos, Universidade de São Paulo, Caixa Postal 369, 13560-970 São Carlos, SP, Brazil*
(Received 11 November 2011; published 31 May 2012)

We present an analytic description of numerical results for the Landau-gauge SU(2) gluon propagator $D(p^2)$, obtained from lattice simulations (in the scaling region) for the largest lattice sizes to date, in $d = 2$, 3 and 4 space-time dimensions. Fits to the gluon data in $3d$ and in $4d$ show very good agreement with the tree-level prediction of the refined Gribov-Zwanziger (RGZ) framework, supporting a massive behavior for $D(p^2)$ in the infrared limit. In particular, we investigate the propagator's pole structure and provide estimates of the dynamical mass scales that can be associated with dimension-two condensates in the theory. In the $2d$ case, fitting the data requires a noninteger power of the momentum p in the numerator of the expression for $D(p^2)$. In this case, an infinite-volume-limit extrapolation gives $D(0) = 0$. Our analysis suggests that this result is related to a particular symmetry in the complex-pole structure of the propagator and *not* to purely imaginary poles, as would be expected in the original Gribov-Zwanziger scenario.

DOI: 10.1103/PhysRevD.85.094513 PACS numbers: 11.15.Ha, 12.38.Aw, 14.70.Dj

I. INTRODUCTION

High-precision data from lattice simulations are a key ingredient in our understanding of the low-energy aspects of Yang-Mills theories associated with color confinement. In fact, whereas new insight into the confinement mechanism may be gained by investigating the properties of gauge-field configurations produced in the simulations (see e.g. [1]), specific features of proposed confinement scenarios may be tested by comparison with lattice data. In this case, one may obtain physical values for a model's parameters by fitting the predicted expression of a given observable to its numerical realization. One may also hope to over-constrain the proposed analytic forms, if the fits can be done with a sufficiently high number and wide range of data points, from which systematic errors have been consistently eliminated. In particular, this applies to predictions for the infrared behavior of gluon and ghost propagators, formulated in Landau gauge for SU(N_c) gauge theory. Here we perform a series of fits to the gluon propagator $D(p^2)$ and test the predictions of the so-called refined Gribov-Zwanziger (RGZ) framework, which differs from the scenario originally proposed by Gribov [2] and Zwanziger [3] through the introduction of dimension-two condensates, associated with dynamical mass generation [4]. Our analysis is done for pure SU(2) gauge theory. The data have been produced previously and discussed in [5–7] (see also [8]), but they have not been systematically fitted until now. A companion paper with similar fits for the ghost propagator is under way [9]. We note that an alternative comparison of these data to analytic predictions was recently presented in [10].

The Gribov-Zwanziger confinement scenario is based on restricting the functional integration to the first Gribov region Ω delimited by the first Gribov horizon $\partial\Omega$, where the smallest nonzero (and positive) eigenvalue of the Faddeev-Popov matrix $\mathcal{M}$ goes to zero [2,3]. Let us recall that limiting the gauge configurations to this region was an attempt—made by Gribov in Ref. [2]—to fix the gauge completely, getting rid of spurious gauge copies, known thereafter as Gribov copies. Now, Ω is a convex region of very high dimensionality and therefore, as the infinite-volume limit is approached, the increase in entropy should favor [11] gauge configurations on the surface $\partial\Omega$. This in turn can cause the infrared enhancement of the ghost propagator (which is related to the inverse of $\mathcal{M}$), inducing long-range effects in the theory. Indeed, in Coulomb gauge, the restriction to the first Gribov region causes the appearance of a confining color-Coulomb potential [2,12]. Thus, in this scenario, formulated for momentum-space propagators, the long-range features needed to explain the color-confinement mechanism are manifest in the ghost propagator, whereas the momentum-space gluon propagator $D(p^2)$ should be *suppressed* in the infrared limit. Such a suppression is associated with violation of spectral positivity, which is commonly interpreted as gluon confinement [3,13,14]. In particular, $D(0)$ is originally expected to be zero [2,3], corresponding to maximal violation of spectral positivity. The parametrization of this behavior as a propagator having a pair of poles with purely imaginary masses has arisen in the Gribov-Zwanziger approach [2,3], in connection with the study of gauge copies.

Lattice studies (see [8] for a recent review) have confirmed the suppression of the gluon propagator in the infrared limit and the enhancement of the ghost propagator

*attilio@ifsc.usp.br
†david.dudal@ugent.be
‡mendes@ifsc.usp.br
§nele.vandersickel@ugent.be

at intermediate momenta. However, considering lattice sizes large enough to allow the investigation of the deep infrared regime, it is clear that the results of the simulations are *not* compatible with the scenario described above. Indeed—in space-time dimension $d = 3$, 4—the gluon propagator shows a finite value as the momentum is taken to zero and the enhancement of the ghost propagator is lost in this limit. We note the very large lattice sizes employed in order to observe such a behavior, $L \approx 20$ fm and larger [5–7,15–18]. In any case, violation of reflection positivity for the real-space gluon propagator (see e.g. [19]) is clearly observed in the data.

Recently, the quantitative description of the massive behavior for the gluon propagator has been studied by several groups [10,18,20–31], based on different proposed analytic forms. Earlier attempts of fitting gluon-propagator data can be found, for example, in Refs. [32–35]. We note that some of these studies (see e.g. [32,35]) have considered the so-called Gribov-Stingl form [36,37] for modeling the massive behavior of the gluon propagator. This form is a generalization of the Gribov propagator described above, including pairs of complex-conjugate poles with a nonzero real part. As illustrated below, the behavior predicted for $D(p^2)$ in the RGZ framework is also based on general complex-conjugate poles for the (massive) propagator. This proposed form is given for SU(N_c) gauge theory and for four or three space-time dimensions [4,38–41]. On the contrary, in the $2d$ case, the RGZ approach cannot be implemented, since the dimension-two condensates would induce severe infrared singularities, precluding the restriction of the functional integration to the first Gribov region [42]. By fitting rational functions of p^2 to the *whole* range of data for the SU(2) gluon propagator, we are able to obtain estimates for the values in physical units for the masses in the RGZ framework, as well as to gain a better understanding of the pole structure in the proposed expressions. In each case, we look for the best fit to the data, with the smallest number of independent parameters, and relate them to the condensates in the proposed analytic forms only at the end. Put differently, the predicted dependence of the fit parameters on the condensates is *not* imposed in the fitting form, but is obtained as a result of the fit. This allows us to use a wide fitting range, considering all data points. We note that predictions from the RGZ framework were already tested in [24], showing good fits (using a somewhat different analytic form and a smaller fitting range) to $4d$ lattice data for the SU(3) case.

The paper is organized as follows. The Gribov-Zwanziger scenario is briefly reviewed in Sec. II. The introduction of condensates as part of the RGZ scenario is summarized is Sec. III, where we present the expressions to be fitted to the lattice data. The numerical results are discussed in general in Sec. IV and, in particular, for the $4d$, $3d$ and $2d$ cases, respectively, in Secs. V, VI, and VII. We present our conclusions in Sec. VIII.

II. THE GRIBOV-ZWANZIGER ACTION

The Gribov-Zwanziger (GZ) action, introduced in 1989 [13], implements an all-order restriction of the path integral to the first Gribov region

$$\Omega \equiv \{A^a_\mu(x):\ \partial_\mu A^a_\mu(x) = 0,\ \mathcal{M}^{ab}(x,y) > 0\}, \tag{1}$$

where $A^a_\mu(x)$ is the gauge field and $\mathcal{M}^{ab}(x,y)$ is the Landau-gauge Faddeev-Popov operator

$$\begin{aligned}\mathcal{M}^{ab}(x,y) &= -\delta(x-y)\partial_\mu D^{ab}_\mu \\ &= \delta(x-y)(-\delta^{ab}\partial^2_\mu + f^{abc}\partial_\mu A^c_\mu).\end{aligned} \tag{2}$$

By introducing auxiliary fields—a pair of complex-conjugate bosonic fields $(\bar\varphi^{ac}_\mu, \varphi^{ac}_\mu)$ and a pair of anticommuting complex-conjugate fields $(\bar\omega^{ac}_\mu, \omega^{ac}_\mu)$—one is able to obtain a local renormalizable action [11,43,44]. More precisely, the generating functional for the GZ action can be written in d space-time dimensions as [13,44,45]

$$Z(J) = \int [d\Phi] \mathrm{e}^{S_{\mathrm{GZ}} + \int d^dx J^a_\mu(x) A^a_\mu(x)}, \tag{3}$$

where S_{GZ} is the local GZ action given by

$$S_{\mathrm{GZ}} = S_0 + S_\gamma, \tag{4}$$

with

$$\begin{aligned}S_0 = S_{\mathrm{YM}} + S_{\mathrm{gf}} + \int d^dx [&\bar\varphi^{ac}_\mu \partial_\nu D^{ab}_\nu \varphi^{bc}_\mu - \bar\omega^{ac}_\mu \partial_\nu (D^{ab}_\nu \omega^{bc}_\mu) \\ &- g(\partial_\nu \bar\omega^{an}_\mu) f^{abc} D^{bm}_\nu c^m \varphi^{cn}_\mu]\end{aligned} \tag{5}$$

and

$$\begin{aligned}S_\gamma = -\gamma^2 g \int d^dx \Big[&f^{abc} A^a_\mu \varphi^{bc}_\mu + f^{abc} A^a_\mu \bar\varphi^{bc}_\mu \\ &+ \frac{d}{g}(N_c^2 - 1)\gamma^2 \Big].\end{aligned} \tag{6}$$

Here, a, b, c, m and n are color indices in the adjoint representation, N_c is the number of colors, γ is the so-called Gribov parameter, S_{YM} is the classical Yang-Mills action

$$S_{\mathrm{YM}} = \frac{1}{4}\int d^dx F^a_{\mu\nu} F^a_{\mu\nu} \tag{7}$$

and S_{gf} is the Landau-gauge-fixing action

$$S_{\mathrm{gf}} = \int d^dx (b^a \partial_\mu A^a_\mu + \bar c^a \partial_\mu D^{ab}_\mu c^b), \tag{8}$$

where the auxiliary field b^a is a Lagrange multiplier enforcing Landau gauge and $(\bar c^a, c^a)$ are the Faddeev-Popov ghost fields. Also, we indicate with $[d\Phi]$ the integration over all fields $\Phi \in \{A^a_\mu, c^a, \bar c^a, b^a, \bar\varphi^{ac}_\mu, \varphi^{ac}_\mu, \omega^{ac}_\mu, \bar\omega^{ac}_\mu\}$. Notice that one can simplify the notation of the auxiliary fields $(\bar\varphi^{ac}_\mu,\ \varphi^{ac}_\mu,\ \bar\omega^{ac}_\mu,\ \omega^{ac}_\mu)$ in the action S_0 using the

symmetry of this action with respect to the composite index $i \equiv (\mu, c)$. Thus, we can set

$$(\bar{\varphi}^{ac}_{\mu}, \varphi^{ac}_{\mu}, \bar{\omega}^{ac}_{\mu}, \omega^{ac}_{\mu}) = (\bar{\varphi}^{a}_{i}, \varphi^{a}_{i}, \bar{\omega}^{a}_{i}, \omega^{a}_{i}) \tag{9}$$

and write

$$S_0 = S_{\mathrm{YM}} + S_{\mathrm{gf}} + \int d^d x [\bar{\varphi}^a_i \partial_\nu (D^{ab}_\nu \varphi^b_i) - \bar{\omega}^a_i \partial_\nu (D^{ab}_\nu \omega^b_i) - g(\partial_\nu \bar{\omega}^a_i) f^{abc} D^{bm}_\nu c^m \varphi^c_i]. \tag{10}$$

Finally, the parameter γ in Eq. (6) is fixed by the so-called gap equation (also known as the horizon condition)

$$\langle g f^{abc} A^a_\mu \varphi^{bc}_\mu \rangle + \langle g f^{abc} A^a_\mu \bar{\varphi}^{bc}_\mu \rangle + 2\gamma^2 d(N_c^2 - 1) = 0, \tag{11}$$

where $\langle\rangle$ indicates the expectation value in the measure defined by Eq. (3). This condition is a consequence of the restriction of the path integral to the first Gribov region.

As mentioned in the Introduction, one of the main outcomes of the GZ theory is the modification of the behavior of gluon and ghost propagators in the infrared (IR) limit in comparison with the perturbative behavior $1/p^2$ [2,3,11,13,14,46]. Indeed, the gluon propagator becomes IR-suppressed with a tree-level behavior given by

$$\langle A^a_\mu(p) A^b_\nu(-p) \rangle \equiv \delta^{ab} D(p^2) \left(\delta_{\mu\nu} - \frac{p_\mu p_\nu}{p^2} \right) = \delta^{ab} \frac{p^2}{p^4 + 2g^2 N_c \gamma^4} \left(\delta_{\mu\nu} - \frac{p_\mu p_\nu}{p^2} \right). \tag{12}$$

This result is confirmed by one-loop calculations [47,48]. The above expression for the gluon propagator implies that $D(p^2)$ is null at zero momentum, which in turn indicates maximal violation of reflection positivity for the real-space gluon propagator $D(x)$ [46]. This violation is usually considered a manifestation of gluon confinement [3,13,14]. At the same time, one finds that the ghost propagator displays an enhanced IR behavior

$$\langle c^a(p) \bar{c}^b(p) \rangle \equiv \delta^{ab} \mathcal{G}(p^2) \sim \delta^{ab} \frac{1}{p^4}. \tag{13}$$

This behavior is indicative of a long-range interaction in the theory and it should be related to quark confinement [2,14,49].

III. THE REFINED GRIBOV-ZWANZIGER FRAMEWORK

More recently, the GZ action has been "refined" by taking into account the possible existence of dimension-two condensates [4,38–41]. In the most general case [41], four different condensates are considered, i.e.

$$\langle A^a_\mu A^a_\mu \rangle \to -m^2 \qquad \langle \bar{\varphi}^a_i \varphi^a_i \rangle \to M^2$$
$$\langle \varphi^a_i \varphi^a_i \rangle \to \rho \qquad \langle \bar{\varphi}^a_i \bar{\varphi}^a_i \rangle \to \rho^\dagger, \tag{14}$$

where we have listed the dynamical mass associated to each condensate. (Note that ρ is complex, whereas $-m^2$ and M^2 are real and positive.) The condensate $-m^2$ is directly related to the gluon condensate $\langle g^2 A^2 \rangle$ (see e.g. [24]). One can show [41] that the refined Gribov-Zwanziger (RGZ) action can be renormalized. At the same time, there is clear evidence that the original GZ theory dynamically transforms into the refined theory, since the minimum of the associated effective potential favors nonvanishing condensates [41]. As displayed below, a nonzero value for these condensates has an effect on the IR behavior of gluon propagators. The influence on the ghost propagator will be discussed in a forthcoming work [9], in which one-loop results are taken into account and the role of the ghost-gluon vertex is investigated.

The gluon propagator

In the presence of the four condensates considered in Eq. (14), the GZ gluon propagator (12) is modified [41] as

$$D(p^2) = \frac{p^4 + 2M^2 p^2 + M^4 - \rho\rho^\dagger}{p^6 + p^4(m^2 + 2M^2) + p^2(2m^2M^2 + M^4 + \lambda^4 - \rho\rho^\dagger) + m^2(M^4 - \rho\rho^\dagger) + M^2\lambda^4 - \frac{\lambda^4}{2}(\rho + \rho^\dagger)}, \tag{15}$$

where the condensates m^2, M^2, ρ are described above and λ^4 is related to the Gribov parameter γ through $\lambda^4 = 2g^2 N_c \gamma^4$. Since ρ and $\rho^\dagger$ are complex-conjugate quantities, we can set

$$\rho = \rho_1 + i\rho_2 \qquad \rho^\dagger = \rho_1 - i\rho_2 \tag{16}$$

and rewrite Eq. (15) as

$$D(p^2) = \frac{p^4 + 2M^2 p^2 + M^4 - (\rho_1^2 + \rho_2^2)}{p^6 + p^4(m^2 + 2M^2) + p^2[2m^2M^2 + M^4 + \lambda^4 - (\rho_1^2 + \rho_2^2)] + m^2[M^4 - (\rho_1^2 + \rho_2^2)] + \lambda^4(M^2 - \rho_1)}. \tag{17}$$

It is interesting to notice that this propagator gets simplified if $\rho = \rho^\dagger = \rho_1$ (i.e. $\rho_2 = 0$), which corresponds to the equality $\langle \bar{\varphi}\,\bar{\varphi} \rangle = \langle \varphi\varphi \rangle$ from (14). Indeed, in this case one can factorize the quantity $p^2 + M^2 - \rho_1$ in the numerator and in the denominator of the above formula, obtaining

$$D(p^2) = \frac{p^2 + M^2 + \rho_1}{p^4 + p^2(M^2 + m^2 + \rho_1) + m^2(M^2 + \rho_1) + \lambda^4}. \quad (18)$$

Clearly, both propagators (17) and (18) have, in principle, a finite *nonzero* value at zero momentum. Nevertheless, if the value of $D(0)$ is sufficiently small, one still finds that the real-space propagator $D(x)$ becomes negative for some (large) value of x, i.e. reflection positivity can also be violated for these propagators.

Note that both Eqs. (17) and (18) can be decomposed as sums of propagators of the type $\alpha/(p^2 + \omega^2)$. In particular, we can write Eq. (17) as

$$D(p^2) = \frac{\alpha}{p^2 + \omega_1^2} + \frac{\beta}{p^2 + \omega_2^2} + \frac{\gamma}{p^2 + \omega_3^2}. \quad (19)$$

To this end, we only need to solve the cubic equation

$$x^3 + x^2(m^2 + 2M^2) + x[2m^2M^2 + M^4 + \lambda^4 - (\rho_1^2 + \rho_2^2)] + m^2[M^4 - (\rho_1^2 + \rho_2^2)] + \lambda^4(M^2 - \rho_1) = 0, \quad (20)$$

obtained by setting $p^2 = x$ in the denominator of Eq. (17), and to find its three roots ω_1^2, ω_2^2 and ω_3^2. At the same time, the gluon propagator in Eq. (18) can be written as

$$D(p^2) = \frac{\alpha_+}{p^2 + \omega_+^2} + \frac{\alpha_-}{p^2 + \omega_-^2}, \quad (21)$$

where we expect to have $\alpha_- = \alpha_+^*$ if $\omega_-^2 = (\omega_+^2)^*$, i.e. if ω_+^2 and ω_-^2 are complex conjugates. Here, $\omega_\pm^2$ are the roots of the quadratic equation

$$x^2 + x(M^2 + m^2 + \rho_1) + m^2(M^2 + \rho_1) + \lambda^4 = 0, \quad (22)$$

obtained by setting $p^2 = x$ in the denominator of Eq. (18). Clearly, one finds complex-conjugate poles if $|M^2 - m^2 + \rho_1| < 2\lambda^2$.

Let us remark that rational forms such as (17) and (18) for the gluon propagator were considered by Stingl [36,37], as a way of accounting for nonperturbative effects in an extended perturbative approach to Euclidean QCD. More precisely, in his treatment, one expresses the proper vertices of the theory as an iterative sequence of functions yielding a self-consistent solution to the Dyson-Schwinger equations. In particular, for the gluon propagator, this sequence is written [see Eq. (2.10) in Ref. [37]] in terms of ratios of polynomials in the variable p^2, of degree r in the numerator and $r + 1$ in the denominator, with $r = 0, 1, 2, \ldots$. This functional form is then related, via operator product expansion, to the possible existence of vacuum condensates of dimension $2n$, with $n \geq 1$. At the same time, the associated complex-conjugate poles[1] are interpreted as short-lived elementary excitations of the gluon field [3,36,37]. By comparison, in the RGZ framework, one proposes specific forms for the dimension-two condensates—related to the auxiliary fields of the GZ action—and then obtains (at tree level) the rational functions in Eqs. (17) and (18), which correspond, respectively, to cases with $r = 3$ and 2 in Stingl's iterative sequence.

In Sec. V below, we show that the simplest rational form [with $r = 2$, corresponding to Eq. (18)] works well in the $4d$ SU(2) case. A similar result was obtained for the SU(3) case in [24].[2] It may be noted that, in Ref. [32], lattice data for the $4d$ SU(3) Landau-gauge gluon propagator were fitted using the above sequence of functions with $r = 2$, 4 and it was found that a good description of the data can be achieved only for $r = 4$. Note, however, that the fit was performed for the real-space propagator, for which the analysis is known to be complicated by several technical issues (see e.g. [19,52]). Moreover, although the lattice volume considered was rather large, the study employed asymmetric lattices, which may give rise to systematic effects [53].

IV. NUMERICAL SIMULATIONS

The data presented here for the SU(2) Landau-gauge gluon propagator were produced in 2007. The $3d$ and $4d$ cases were run on the 4.5 Tflops IBM supercomputer at LCCA–USP [54], whereas the $2d$ case was run on various PC clusters at the IFSC–USP. Most of these data have already been discussed in Refs. [5–8], but they were not systematically fitted up to now.

In the $4d$ case, we have considered lattice sides $N = 48$, 56, 64, 80, 96 and 128, with lattice parameter $\beta = 2.2$. The corresponding lattice spacing a is approximately 0.210 fermi, implying that the smallest nonzero momentum $p_{\min} = 2\sin(\pi/N)$ is about 46 MeV in physical units for the $N = 128$ lattice. In this case, the physical lattice volume $V = N^4$ is about (27 fermi)^4. The number of gauge-field configurations produced was 168 for $N = 128$ and about 250 for the other lattice sizes.

In $3d$, we have $N = 140$, 200, 240 and 320 at $\beta = 3.0$, with $a \approx 0.268$ fermi. Then, for the lattice volume 320^3 the smallest nonzero momentum $p_{\min}$ is about 14 MeV and the physical volume corresponds to about (85 fermi)^3. The number of configurations was 630, 525, 350 and 125, respectively, for the four lattice sizes.

Finally, in the two-dimensional case, we considered $N = 80$, 120, 160, 200, 240, 280 and 320 at $\beta = 10.0$. In this case the lattice spacing is about 0.219 fermi, the lattice volumes 320^2 correspond to $V \approx (70 \text{ fermi})^2$ and in this case $p_{\min} \approx 18$ MeV. We have about 600 configurations for each lattice volume.

In all cases we set the lattice spacing a by considering the input value $\sigma^{1/2} = 0.44$ GeV for the string tension,

[1] See [37,50,51] for some considerations concerning the issue of causality for propagators with complex poles.

[2] Let us mention that the condensate ρ was not considered in Ref. [24]. Therefore, when discussing fit results using Eq. (18), we must compare their values for M^2 to our values for $M^2 + \rho_1$.

which is a typical value for this quantity in the $4d$ SU(3) case. The evaluation of the lattice string tension is described in [35,55,56], respectively, for $d = 2$, 3 and 4. Note that all our runs are in the scaling region [35,56,57] and all data refer to the SU(2) case. Possible systematic effects due to Gribov copies [58–62] as well as unquenching effects [63–66] were *not* considered here. Finite-volume effects, on the other hand, are well under control. In particular, in $3d$ and in $4d$, our largest lattice volumes can be already considered as infinite. In the $2d$ case, a simple extrapolation to infinite volume needs to be considered, as done in Sec. VII to obtain the limiting value of $D(0)$.

Configurations have been generated by alternating heat-bath updates of the link variables with micro-canonical steps, in order to reduce the problem of critical slowing-down (see for example [67] and references therein). Gauge-fixing to Landau gauge was done using the stochastic overrelaxation algorithm [55,67]. Let us also recall [see Eq. (12)] that the gluon propagator $D(p^2)$ in Landau gauge is evaluated using

$$D^{bc}_{\mu\nu}(p) = \sum_{x,y} \frac{e^{-2\pi i \hat{p}\cdot(x-y)/N}}{V} \langle A^b_\mu(x) A^c_\nu(y)\rangle = \delta^{bc}\left(g_{\mu\nu} - \frac{p_\mu p_\nu}{p^2}\right) D(p^2). \tag{23}$$

Here $A^b_\mu(x)$ is the lattice gluon field defined as[3]

$$A_\mu(x) = \frac{1}{2i}[U_\mu(x) - U^\dagger_\mu(x)], \tag{24}$$

where $U_\mu(x)$ are the usual link variables of the Wilson action. Also, the momentum components p_μ are given by

$$p_\mu = 2\sin\left(\frac{\pi \hat{p}_\mu}{N}\right) \tag{25}$$

and $\hat{p}_\mu$ takes values $0, 1, N-1$.

In $2d$ we considered momenta with components $(p, 0)$ and (p, p), plus all possible permutations of the components. Similarly, in $3d$, we have data for momenta with components $(p, 0, 0)$, $(p, p, 0)$ and (p, p, p) and all possible permutations of components. Finally, in $4d$, we evaluated the propagator for momenta with components $(p, 0, 0, 0)$, $(p, p, 0, 0)$, $(p, p, p, 0)$ and (p, p, p, p). In this case, we considered all possible permutations of the components for momenta of the type $(p, 0, 0, 0)$. On the contrary, we did not consider permutations for the momenta $(p, p, p, 0)$ and in the case $(p, p, 0, 0)$ we allowed all permutations satisfying the constraint $p_4 = 0$. When permutations of the momentum components were available, an average over the different permutations was taken for each configuration. In order to reduce discretization effects—and, in particular, those related to the breaking of rotational symmetry [33,69,70]—we have considered, in addition to the usual (unimproved) momentum defined by the squared magnitude of the lattice momenta

$$p^2 = \sum_\mu p^2_\mu, \tag{26}$$

the improved definition [69]

$$p^2 = \sum_\mu p^2_\mu + \frac{1}{12}\sum_\mu p^4_\mu. \tag{27}$$

This definition does not affect the value of p^2 in the IR limit, but modifies its value significantly for large momenta. In particular, the largest value of p^2—obtained when $\hat{p}_\mu = N/2$ in Eq. (25) for all directions μ—is given (in lattice units, for the d-dimensional case), by $4d$ if the unimproved definition is considered, and by $16d/3$ in the improved case. For the β values considered here, this implies that the largest momentum $p_{\max}$ is about 2.54, 2.55 and 3.75 GeV, respectively, in $2d$, $3d$ and $4d$ in the unimproved case, and about 2.94, 2.94 and 4.33 GeV using improved momenta.

In the next sections we present fits (obtained using `gnuplot`) of the $4d$, $3d$ and $2d$ data for the SU(2) gluon propagator and compare the fit results to the predictions of the RGZ action, discussed above in Sec. . We remark that the shown data for $D(p^2)$ are *not* normalized. Note that a (multiplicative) renormalization condition at a given scale μ^2 would simply correspond to a rescaling of the overall factor C in the fitting forms considered below. The condensates and the poles, on the other hand, are not affected by such a renormalization.[4] We also note that, whenever possible, we avoid rounding off the values of the fit parameters. On the contrary, values for the associated physical quantities (i.e. condensates and poles) are rounded to show errors with one significant digit only. We refer to the `gnuplot` documentation ([71] "Statistical Overview" section) for information on the significance of the standard errors calculated for the fit parameters.

V. THE 4D CASE

As a first attempt in the $4d$ case, we consider a fitting function of the simplest Gribov-Stingl form[5]

[3]With this definition of the lattice gluon field, the gluon propagator evaluated on the lattice corresponds to the propagator $g^2 D(p^2)$ in the continuum, which has mass dimension $2 - d$ in the d-dimensional case [68].

[4]Of course, condensates are, in general, renormalization-scale- and renormalization-scheme-dependent quantities. This dependence is not taken into account here because the fitting forms we use are inspired by a tree-level propagator. Indeed, in order to consider these effects, analytic results beyond tree-level computations must be employed.

[5]Since our largest momentum is of the order of 4 GeV, ultraviolet logarithmic corrections are not important to describe the lattice data and they are not included in the fitting functions proposed here. This also avoids the problem of having to regularize the corresponding Landau pole by hand.

TABLE I. Fits of the gluon-propagator data in the 4*d* case, for different lattice volumes, using the fitting function $f_1(p^2)$ in Eq. (28) and unimproved momenta [see Eq. (26)]. We report, besides the value of the fit parameters, the χ^2/d.o.f. obtained in each case. The whole range of momenta was considered for the fit. Errors shown in parentheses correspond to one standard deviation.

V	C	u(GeV)	t(GeV^2)	s(GeV^2)	χ^2/d.o.f.
48^4	0.567 (0.016)	0.507 (0.065)	0.607 (0.023)	2.417 (0.269)	16.47
56^4	0.572 (0.014)	0.495 (0.058)	0.602 (0.021)	2.344 (0.234)	15.46
64^4	0.566 (0.013)	0.522 (0.052)	0.612 (0.019)	2.452 (0.223)	15.00
80^4	0.562 (0.012)	0.496 (0.048)	0.612 (0.017)	2.443 (0.199)	16.59
96^4	0.567 (0.011)	0.484 (0.044)	0.604 (0.016)	2.367 (0.178)	15.96
128^4	0.560 (0.010)	0.534 (0.037)	0.621 (0.014)	2.553 (0.166)	10.65

TABLE II. Fits of the gluon-propagator data in the 4*d* case, for different lattice volumes, using the fitting function $f_1(p^2)$ in Eq. (28) and improved momenta [see Eq. (27)]. We report, besides the value of the fit parameters, the χ^2/d.o.f. obtained in each case. The whole range of momenta was considered for the fit. Errors shown in parentheses correspond to one standard deviation.

V	C	u(GeV)	t(GeV^2)	s(GeV^2)	χ^2/d.o.f.
48^4	0.791 (0.007)	0.755 (0.027)	0.707 (0.013)	2.419 (0.119)	2.09
56^4	0.801 (0.006)	0.734 (0.023)	0.696 (0.012)	2.305 (0.100)	1.92
64^4	0.791 (0.007)	0.760 (0.024)	0.710 (0.012)	2.425 (0.108)	2.35
80^4	0.785 (0.005)	0.734 (0.019)	0.708 (0.009)	2.404 (0.084)	2.04
96^4	0.795 (0.004)	0.717 (0.016)	0.694 (0.008)	2.291 (0.068)	1.66
128^4	0.784 (0.005)	0.768 (0.017)	0.720 (0.009)	2.508 (0.078)	1.63

$$f_1(p^2) = C\frac{p^2 + s}{p^4 + u^2p^2 + t^2}, \tag{28}$$

which corresponds to the RGZ propagator in Eq. (18), modulo a global rescaling factor C. We note that, in order to improve the stability of the fit, we impose some parameters to be positive, by setting them to be squares. The results of the fit for all lattice volumes, using unimproved and improved momenta, are reported, respectively, in Tables I and II. From the χ^2/d.o.f. values one clearly concludes that the use of improved momenta makes the behavior of the gluon propagator smoother, allowing a better fit to the data. This is also seen by comparing the data in Figs. 1 and 2, plotted, respectively, for unimproved and improved momenta. Let us stress that we are fitting the whole momentum range available and that, for the largest lattice volume, we have 257 data points.

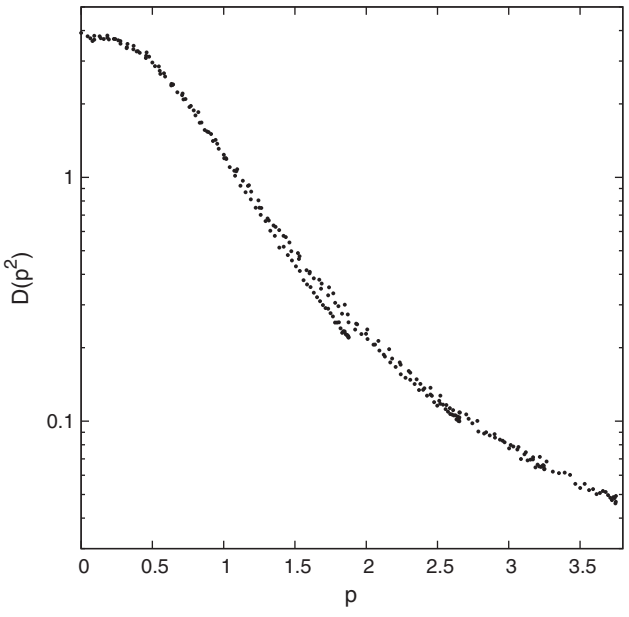

FIG. 1. Plot of the 4*d* gluon propagator $D(p^2)$ (in GeV^{-2}) as a function of the (unimproved) momentum p (in GeV) for the lattice volume $V = 128^4$. As a consequence of the breaking of rotational invariance, the data do not produce a smooth curve. Note the logarithmic scale on the y axis.

In order to extract the value of the condensates described in Sec. above, we now consider only the fit results for the volume $V = 128^4$ (using improved momenta), reported in the last row of Table II. The corresponding plot is shown in Fig. 2. By setting $f_1(p^2)$ equal to the RGZ propagator in Eq. (18) (modulo the global factor C) and using propagation of error, we find for the condensates the values reported in the first column of Table III. (Note that, for this fitting form, the condensates M^2 and ρ_1 cannot be determined separately.) Let us mention that the values obtained here for $M^2 + \rho_1$, m^2 and λ^4 are in good quantitative agreement with the corresponding values—respectively indicated with M^2, m^2 and $2g^2N\gamma^4$—reported in Ref. [24] for the SU(3) case.[6] Also, as remarked above,

[6]For comparison with our values in Table III, the SU(3) condensates from [24] are respectively 2.15(13) GeV^2, $-1.81(14)$ GeV^2 and 4.16(38) GeV^4.

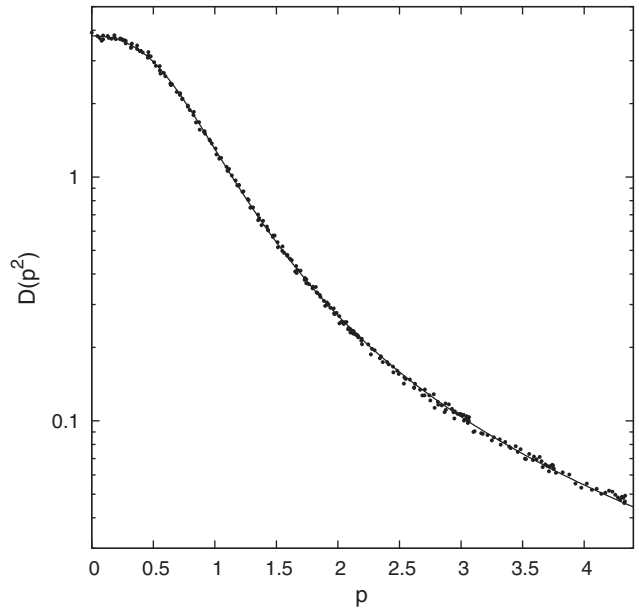

FIG. 2. Plot of the $4d$ gluon propagator $D(p^2)$ (in GeV^{-2}) as a function of the (improved) momentum p (in GeV) for the lattice volume $V = 128^4$. We also show the fitting function $f_1(p^2)$ [see Eq. (28)] with the parameters reported in the last row of Table II. Note the logarithmic scale on the y axis.

the condensate m^2 may be used to obtain a value for the gluon condensate $\langle g^2 A^2 \rangle$, through the relation (see e.g. [24])

$$\langle g^2 A^2 \rangle = -\frac{9}{13}\frac{N_c^2 - 1}{N_c} m^2. \tag{29}$$

In our case, the value $m^2 = -1.92(9)$ from Table III (using propagation of error) yields $\langle g^2 A^2 \rangle = 1.99(9)\ \mathrm{GeV}^2$.

Furthermore, we verify from Table III that $|M^2 - m^2 + \rho_1| < 2\lambda^2$, justifying our expectation (see end of Sec.) that the propagator may be decomposed in terms of a pair of complex-conjugate poles. We can thus write [see Eq. (21)]

TABLE III. Estimates of the parameters of the RGZ gluon propagator in Eq. (18) from fits (see last row of Table II above) to the equivalent form $f_1(p^2)$ in Eq. (28), using propagation of error. For comparison, we also report a Monte Carlo error analysis with 10 000 samples and a bootstrap analysis (fit results given in the text) with 500 samples. In all cases we considered the volume $V = 128^4$ and improved momenta. Errors shown in parentheses correspond to one standard deviation.

parameter	propagation of error	Monte Carlo analysis	bootstrap analysis
$M^2 + \rho_1$ (GeV^2)	2.51(8)	2.51(8)	2.3(3)
m^2 (GeV^2)	−1.92(9)	−1.92(9)	−1.7(2)
λ^4 (GeV^4)	5.3(9)	5.3(4)	4.5(9)

TABLE IV. Estimates of the parameters of the function $f_2(p^2)$ [see Eq. (30)] from fits (see last row of Table II above) to the equivalent form $f_1(p^2)$ in Eq. (28), using propagation of error. For comparison, we also report a Monte Carlo error analysis with 10000 samples and a bootstrap analysis (fit results given in the text) with 500 samples. In all cases we considered the volume $V = 128^4$ and improved momenta. Errors shown in parentheses correspond to one standard deviation.

parameter	propagation of error	Monte Carlo analysis	bootstrap analysis
a	0.392(3)	0.392(2)	0.38(1)
b	1.32(7)	1.32(5)	1.20(7)
v (GeV^2)	0.29(2)	0.29(2)	0.29(3)
w (GeV^2)	0.66(2)	0.66(1)	0.64(2)

$$f_2(p^2) = \frac{\alpha_+}{p^2 + \omega_+^2} + \frac{\alpha_-}{p^2 + \omega_-^2} = \frac{2ap^2 + 2(av + bw)}{p^4 + 2vp^2 + v^2 + w^2}, \tag{30}$$

with $\alpha_\pm = a \pm ib$ and $\omega_\pm^2 = v \pm iw$. The results for the parameters a, b, v and w (again using propagation of error) are shown in the first column of Table IV. Thus, the poles are complex conjugates whose imaginary part is more than twice their real part. We recall that a Gribov propagator would have a null real part.

In order to have better control of the errors on the values of the condensates and poles, we have redone the estimates described above using a Monte Carlo error analysis (with 10 000 samples).[7] The corresponding results are reported in the second columns of Table III and Table IV. Finally, we repeated the fit and the evaluation of the condensates and poles using a bootstrap analysis (with 500 samples). In this case, from the fit of $f_1(p^2)$ [see Eq. (28)] at $V = 128^4$, we find the parameters

$$C = 0.762 \pm 0.024 \tag{31}$$

$$u = 0.755 \pm 0.035\ \mathrm{GeV} \tag{32}$$

$$t = 0.698 \pm 0.027\ \mathrm{GeV}^2 \tag{33}$$

$$s = 2.292 \pm 0.253\ \mathrm{GeV}^2. \tag{34}$$

The corresponding results for the condensates and poles of the propagator are shown in the third columns of Tables III and IV. Clearly, all results obtained agree within one standard deviation.

As a second test, we have also tried to allow for the more general form of the propagator, given in Eq. (17). To this end, we consider the fitting function

[7] To this end, we considered independent Gaussian distributions for the fit parameters. Thus, this Monte Carlo analysis may be considered as a numerical check of the analytic propagation of error.

TABLE V. Fits of the gluon-propagator data in the $4d$ case, for different lattice volumes, using the fitting function $f_3(p^2)$ in Eq. (35) and improved momenta [see Eq. (27)]. We report, besides the value of the fit parameters, the χ^2/d.o.f. obtained in each case. The whole range of momenta was considered for the fit. Errors shown in parentheses correspond to one standard deviation.

V	C	d(GeV^4)	e(GeV^3)	b(GeV^4)	c(GeV^2)	a(GeV)	χ^2/d.o.f.
48^4	0.889 (0.087)	7.742 (9.663)	2.469 (1.651)	26.613 (32.940)	9.692 (13.240)	2.085 (1.143)	1.95
56^4	0.798 (0.007)	0.495 (0.020)	0.055 (0.045)	0.014 (0.023)	0.581 (0.057)	1.093 (0.030)	2.04
64^4	0.795 (0.010)	0.625 (0.662)	0.336 (0.868)	0.543 (2.790)	0.733 (1.031)	1.121 (0.209)	2.52
80^4	0.781 (0.006)	0.514 (0.016)	0.059 (0.037)	0.016 (0.020)	0.593 (0.046)	1.122 (0.025)	2.08
96^4	0.893 (0.104)	10.539 (14.750)	3.036 (2.233)	39.289 (53.150)	16.558 (24.490)	2.720 (1.693)	1.56
128^4	0.784 (0.006)	0.578 (2.192)	0.229 (4.228)	0.253 (9.335)	0.691 (3.795)	1.143 (0.843)	1.69

TABLE VI. Fits of the gluon-propagator data in the $4d$ case, for different lattice volumes, using the fitting function $f_4(p^2)$ in Eq. (36) and improved momenta [see Eq. (27)]. We report, besides the value of the fit parameters, the χ^2/d.o.f. obtained in each case. The whole range of momenta was considered for the fit. Errors shown in parentheses correspond to one standard deviation.

V	C	u(GeV)	t(GeV^2)	s(GeV^2)	k(GeV^2)	χ^2/d.o.f.
48^4	0.802 (0.009)	0.686 (0.081)	0.792 (0.030)	1.662 (0.368)	0.547 (0.149)	2.02
56^4	0.809 (0.008)	0.694 (0.063)	0.761 (0.034)	1.714 (0.365)	0.622 (0.177)	1.89
64^4	0.802 (0.008)	0.701 (0.071)	0.790 (0.028)	1.716 (0.346)	0.573 (0.144)	2.28
80^4	0.793 (0.007)	0.703 (0.046)	0.767 (0.031)	1.882 (0.308)	0.668 (0.154)	2.01
96^4	0.804 (0.006)	0.673 (0.043)	0.757 (0.022)	1.694 (0.246)	0.625 (0.119)	1.62
128^4	0.793 (0.006)	0.727 (0.045)	0.791 (0.025)	1.903 (0.265)	0.631 (0.120)	1.60

$$f_3(p^2) = C\frac{p^4 + 2a^2p^2 + b}{p^6 + cp^4 + dp^2 + e^2}, \tag{35}$$

which has six parameters. As can be seen in Table V, the values of χ^2/d.o.f. do not improve in comparison with the previous (4-parameter) fit and, with the exception of the global factor C, most of the parameters are determined with very large errors. This suggests that the above function has too many (redundant) parameters, making the fitting procedure quite unstable. Next, we reduce the number of parameters by one and introduce a general form that will prove useful in the description of the $3d$ data, in Sec. VI. More precisely, we test the fitting function

$$f_4(p^2) = C\frac{(p^2 + s)(p^2 + 1)}{(p^4 + u^2p^2 + t^2)(p^2 + k)} = C\frac{p^4 + (s + 1)p^2 + s}{p^6 + (k + u^2)p^4 + (ku^2 + t^2)p^2 + kt^2}. \tag{36}$$

This function is of the type (35) (with different parameters), but is written as a simple generalization of $f_1(p^2)$ in Eq. (28).[8] Fit results are shown in Table VI. In this case the fits look reasonable. The corresponding values for the condensates and λ^4 in Eq. (17) are obtained by a Monte Carlo analysis (with 10 000 samples) using the data in the last row of Table VI. We note that, in this case, the fitting form allows us to evaluate M^2, ρ_1 and $|\rho|$ separately. We find the values

$$M^2 = 1.5 \pm 0.1 \text{ GeV}^2 \tag{37}$$

$$m^2 = -1.7 \pm 0.3 \text{ GeV}^2 \tag{38}$$

$$\lambda^4 = 4.1 \pm 1.0 \text{ GeV}^4 \tag{39}$$

$$\rho_1 = 0.5 \pm 0.1 \text{ GeV}^2 \tag{40}$$

$$\rho_1^2 + \rho_2^2 = 0.2 \pm 0.1 \text{ GeV}^2. \tag{41}$$

We see that the errors are larger, and that the value of $M^2 + \rho_1$ is incompatible with the numbers in Table III (obtained assuming $\rho_2 = 0$). Also, a comparison of the values in (40) and (41) suggests a very small (and imaginary) value for ρ_2, implying that ρ is real and thus supporting the simpler form in Eq. (18), fitted above using the function $f_1(p^2)$. Moreover, the χ^2/d.o.f. is not better for the 5-parameter fit compared to the 4-parameter fit, indicating that the latter is more stable.

We thus conclude that our best fit is $f_1(p^2)$ in Eq. (28), i.e. the $4d$ gluon-propagator lattice data favor the simplified expression in Eq. (18), implying $\langle\bar{\varphi}\,\bar{\varphi}\rangle = \langle\varphi\varphi\rangle$.

VI. THE 3*D* CASE

In this case the simplified fitting form $f_1(p^2)$ in Eq. (28) is not able to describe well the lattice data. Indeed, even using improved momenta (see Table VII), the χ^2/d.o.f.

[8]Note that a fit using the more general form in Eq. (42) below is unstable in this case, yielding large errors for the fit parameters. Nevertheless, this fit suggests the factor $(p^2 + 1)$ in the numerator of (36), as adopted here.

TABLE VII. Fits of the gluon-propagator data in the $3d$ case, for different lattice volumes, using the fitting function $f_1(p^2)$ in Eq. (28) and improved momenta [see Eq. (27)]. We report, besides the value of the fit parameters, the χ^2/d.o.f. obtained in each case. The whole range of momenta was considered for the fit. Errors shown in parentheses correspond to one standard deviation.

V	C(GeV)	u(GeV)	t(GeV^2)	s(GeV^2)	χ^2/d.o.f.
140^3	0.441 (0.003)	0.306 (0.013)	0.385 (0.009)	0.217 (0.013)	10.86
200^3	0.440 (0.002)	0.305 (0.011)	0.389 (0.008)	0.223 (0.011)	8.68
240^3	0.443 (0.002)	0.307 (0.010)	0.374 (0.007)	0.198 (0.009)	6.53
320^3	0.445 (0.002)	0.296 (0.011)	0.365 (0.006)	0.183 (0.008)	3.19

values obtained are quite large. Moreover, as can be seen in Fig. 3, the fit clearly fails in the IR region.[9] The situation improves by considering the (5-parameter) fitting function $f_4(p^2)$ in Eq. (36) above, as can be seen from the results reported in Tables VIII and IX, obtained, respectively, using unimproved and improved momenta. Note that, as in the $4d$ case, the use of improved momenta helps to obtain a better fit to the data.

One can also try to use the more general function

$$f_5(p^2) = C\frac{(p^2+s)(p^2+l)}{(p^4+u^2p^2+t^2)(p^2+k)}, \tag{42}$$

obtained by introducing the extra parameter l. In this case, the results of the fit using improved momenta for the lattice volume $V = 320^3$ are

$$C = 0.405 \pm 0.003 \text{ GeV} \tag{43}$$

$$u = 0.692 \pm 0.040 \text{ GeV} \tag{44}$$

$$t = 0.635 \pm 0.018 \text{ GeV}^2 \tag{45}$$

$$s = 0.025 \pm 0.002 \text{ GeV}^2 \tag{46}$$

$$k = 0.050 \pm 0.007 \text{ GeV}^2 \tag{47}$$

$$l = 1.092 \pm 0.103 \text{ GeV}^2 \tag{48}$$

with χ^2/d.o.f. $= 1.19$. By noticing that $l \approx 1$ and by comparing these values to the corresponding ones from the fit using $f_4(p^2)$ in Eq. (36) (reported in the last row of Table IX), it is clear that the two results are equivalent. At any rate, the values of χ^2/d.o.f. for the 6-parameter fit [using the function $f_5(p^2)$ in Eq. (42)] and for the fit in Table IX are the same, indicating that the latter is more stable.

In order to evaluate the condensates of the RGZ model, we thus consider only the results from the fit using $f_4(p^2)$, given for the lattice size $N = 320$ in the last row of Table IX. (The corresponding plot is shown in Fig. 4.) By setting $f_4(p^2)$ [see Eq. (36)] equal to the RGZ propagator (17) modulo the global factor C, we find (using propagation of error) the values for the condensates reported in the first column of Table X. Note that, using this fitting form, we are able to evaluate M^2, ρ_1 and $|\rho|$ (and therefore ρ_2) separately. In this case, we can see that $\rho_2 \neq 0$ and ρ is indeed a complex quantity. This is consistent with the fact that the (four-parameter) fit to the simplified form $f_1(p^2)$ fails, as seen above.

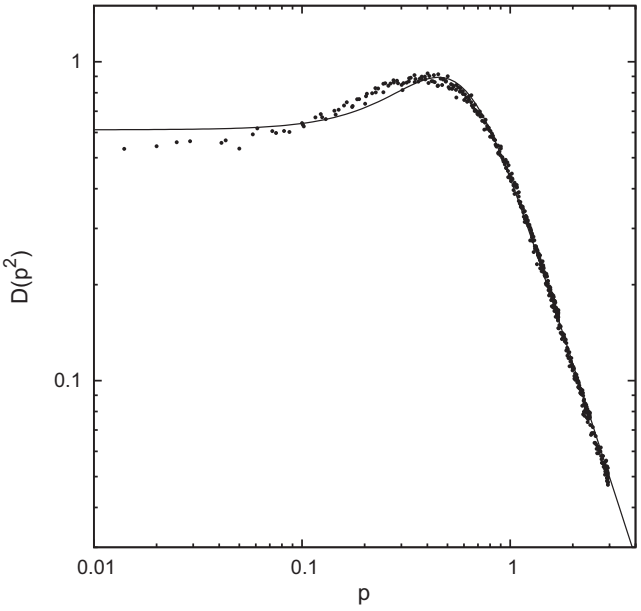

FIG. 3. Plot of the $3d$ gluon propagator $D(p^2)$ (in GeV^{-1}) as a function of the (improved) momentum p (in GeV) for the lattice volume $V = 320^3$. We also show the fitting function $f_1(p^2)$ [see Eq. (28)] with the parameters reported in the last row of Table VII. Note the logarithmic scale on both axes.

Finally, we decompose the propagator as in Eq. (19) with $\beta = a + ib$, $\gamma = a - ib$, $\omega_2^2 = v + iw$ e $\omega_3^2 = v - iw$, i.e. we consider the function

$$f_6(p^2) = \frac{\alpha}{p^2+\omega_1^2} + \frac{2ap^2 + 2(av+bw)}{p^4 + 2vp^2 + v^2 + w^2}. \tag{49}$$

We find (again using propagation of error) the results[10] reported in the first column of Table XI. Note that the imaginary part w of the complex-conjugate poles is more

[9] In order to highlight the results at small momenta, here and in Fig. 4 we present the plot with a logarithmic scale on both axes.

[10] Clearly, we have $\omega_1^2 = k$ from $f_4(p^2)$.

TABLE VIII. Fits of the gluon-propagator data in the $3d$ case, for different lattice volumes, using the fitting function $f_4(p^2)$ in Eq. (36) and unimproved momenta [see Eq. (26)]. We report, besides the value of the fit parameters, the χ^2/d.o.f. obtained in each case. The whole range of momenta was considered for the fit. Errors shown in parentheses correspond to one standard deviation.

V	C(GeV)	u(GeV)	t(GeV^2)	s(GeV^2)	k(GeV^2)	χ^2/d.o.f.
140^3	0.289 (0.002)	0.382 (0.022)	0.552 (0.006)	0.018 (0.003)	0.030 (0.006)	10.48
200^3	0.289 (0.002)	0.386 (0.019)	0.552 (0.006)	0.019 (0.003)	0.032 (0.006)	9.45
240^3	0.290 (0.002)	0.393 (0.017)	0.550 (0.005)	0.020 (0.003)	0.034 (0.005)	6.55
320^3	0.290 (0.002)	0.389 (0.017)	0.549 (0.005)	0.019 (0.003)	0.035 (0.005)	2.89

TABLE IX. Fits of the gluon-propagator data in the $3d$ case, for different lattice volumes, using the fitting function $f_4(p^2)$ in Eq. (36) and improved momenta [see Eq. (27)]. We report, besides the value of the fit parameters, the χ^2/d.o.f. obtained in each case. The whole range of momenta was considered for the fit. Errors shown in parentheses correspond to one standard deviation.

V	C(GeV)	u(GeV)	t(GeV^2)	s(GeV^2)	k(GeV^2)	χ^2/d.o.f.
140^3	0.407 (0.001)	0.654 (0.008)	0.623 (0.004)	0.022 (0.002)	0.041 (0.003)	2.14
200^3	0.407 (0.001)	0.655 (0.007)	0.623 (0.004)	0.024 (0.002)	0.043 (0.003)	1.92
240^3	0.408 (0.001)	0.662 (0.007)	0.620 (0.004)	0.025 (0.002)	0.047 (0.003)	1.59
320^3	0.408 (0.001)	0.656 (0.008)	0.619 (0.005)	0.023 (0.002)	0.046 (0.004)	1.19

than twice the value of their real part v, as in the $4d$ case. Note also that the mass ω_1 and the residue α associated with the real pole are very small. Moreover, α is negative, which may be associated with violation of reflection positivity, indicating that this mass cannot correspond to a physical degree of freedom.

Also in this case we have repeated the analysis using a Monte Carlo estimate for the errors (with 10 000 samples) and the bootstrap method (with 500 samples). The results are shown, respectively, in the second and in the third columns of Tables X and XII. The values of the fit parameters for the function (36) using the bootstrap method for the lattice volume $V = 320^3$ are

$$C = 0.411 \pm 0.004 \text{ GeV} \tag{50}$$

$$u = 0.673 \pm 0.016 \text{ GeV} \tag{51}$$

$$t = 0.611 \pm 0.006 \text{ GeV}^2 \tag{52}$$

$$s = 0.025 \pm 0.002 \text{ GeV}^2 \tag{53}$$

$$k = 0.052 \pm 0.005 \text{ GeV}^2, \tag{54}$$

which should be compared to the results shown in the last row of Table IX. Again, all results obtained using the three different analyses agree within one standard deviation.

We thus conclude that, in the $3d$ case, the data support a gluon propagator given by the general RGZ form (17), in which the condensate ρ is a complex quantity. This is in contrast with the $4d$ case seen in the previous section, for which ρ was real. There are also significant differences for the values of the other condensates and of λ^4 in comparison with the $4d$ case. The masses from the complex-conjugate poles, on the contrary, have similar values in $3d$ and $4d$ (see Tables XI and IV respectively).

VII. THE 2*D* CASE

In the two-dimensional case the situation is different. Indeed, we know from Refs. [6,57,72] that the gluon propagator at zero momentum $D(0)$ does go to zero in the infinite-volume limit, even though one always has $D(0) > 0$ at finite lattice volume. Moreover, the behavior of $D(p^2)$ at small momenta is of the type p^η, with some noninteger power $\eta \approx 0.8$. This makes the fitting procedure more complicated than in the above cases, for which polynomial forms were used. After trying several generalizations of the fitting functions considered in the $4d$ and $3d$ cases, we found that a good fit to the gluon data can be obtained using the function

$$f_7(p^2) = C\frac{p^2 + lp^\eta + s}{p^4 + u^2p^2 + t^2}, \tag{55}$$

which is a simple generalization of Eq. (28). Results of the fit for the various lattice volumes, using unimproved and improved momenta, are reported in Tables XII and XIII respectively.[11] A plot of the fit for the lattice volume $V = 320^2$ using improved momenta can be seen in Fig. 5.

It is interesting to note that the function $f_7(p^2)$ above can be decomposed as

[11]Note that in this case the use of improved momenta does not affect the quality of the fit significantly. Nevertheless, we choose to consider improved momenta in our analysis also in $2d$.

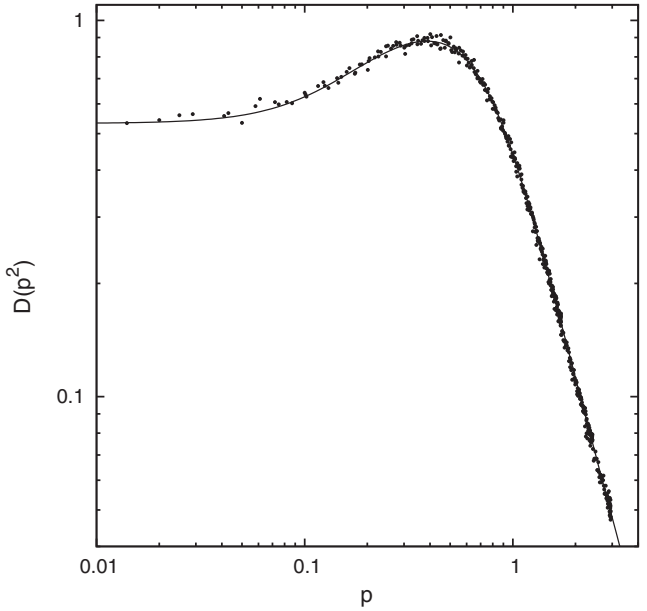

FIG. 4. Plot of the $3d$ gluon propagator $D(p^2)$ (in GeV^{-1}) as a function of the (improved) momentum p (in GeV) for the lattice volume $V = 320^3$. We also show the fitting function $f_4(p^2)$ [see Eq. (36)] with the parameters reported in the last row of Table IX. Note the logarithmic scale on both axes.

$$f_8(p^2) = \frac{\alpha_+(p^2)}{p^2+\omega_+^2} + \frac{\alpha_-(p^2)}{p^2+\omega_-^2} = \frac{2ap^2 + 2cwp^\eta + 2(a\upsilon + bw)}{p^4 + 2\upsilon p^2 + \upsilon^2 + w^2}, \quad (56)$$

with

$$\alpha_\pm(p^2) = a \pm i(b + cp^\eta), \qquad \omega_\pm^2 = \upsilon \pm iw. \quad (57)$$

An estimate for these five parameters is reported in Table XIV, using again three different analyses for the error. The average values of the fit parameters in Eq. (55) using the bootstrap method for the lattice volume $V = 320^2$ are

TABLE X. Estimates of the parameters of the RGZ propagator in Eq. (17) from fits (see last row of Table IX above) to the equivalent form $f_4(p^2)$ in Eq. (36). Errors are obtained using propagation of error, a Monte Carlo analysis with 10 000 samples and a bootstrap analysis with 500 samples. In all cases we considered the volume $V = 320^3$ and improved momenta. Errors shown in parentheses correspond to one standard deviation.

parameter	propagation of error	Monte Carlo analysis	bootstrap analysis
M^2 (GeV^2)	0.512 (1)	0.512 (1)	0.513 (1)
m^2 (GeV^2)	−0.55(1)	−0.55(1)	−0.52(2)
λ^4 (GeV^4)	0.94 (1)	0.94 (1)	0.91 (3)
ρ_1 (GeV^2)	0.479 (2)	0.479 (2)	0.477 (2)
ρ_2 (GeV^2)	0.09 (1)	0.094 (9)	0.100 (6)

TABLE XI. Estimates of the parameters of the function $f_6(p^2)$ [see Eq. (49)] from fits (see last row of Table IX above) to the equivalent form $f_4(p^2)$ in Eq. (36). Errors are obtained using propagation of error, a Monte Carlo analysis with 10 000 samples and a bootstrap analysis with 500 samples. In all cases we considered the volume $V = 320^3$ and improved momenta. Errors shown in parentheses correspond to one standard deviation.

parameter	propagation of error	Monte Carlo analysis	bootstrap analysis
α (GeV)	−0.024(5)	−0.024(5)	−0.029(4)
ω_1^2 (GeV^2)	0.046 (4)	0.046 (4)	0.046 (4)
a (GeV)	0.216 (3)	0.216 (2)	0.220 (4)
b (GeV)	0.27 (5)	0.271 (3)	0.275 (3)
υ (GeV^2)	0.215 (5)	0.215 (5)	0.23 (1)
w (GeV^2)	0.580 (6)	0.580 (6)	0.57 (1)

$$C = 0.112 \pm 0.001\ \mathrm{GeV}^2 \quad (58)$$

$$u = 0.550 \pm 0.013\ \mathrm{GeV} \quad (59)$$

$$t = 0.255 \pm 0.006\ \mathrm{GeV}^2 \quad (60)$$

$$s = 0.0152 \pm 0.0008\ \mathrm{GeV}^2 \quad (61)$$

$$l = 0.326 \pm 0.033\ \mathrm{GeV}^{2-\eta} \quad (62)$$

$$\eta = 0.859 \pm 0.026. \quad (63)$$

We also tried an extrapolation to the infinite-volume limit of the gluon propagator at zero momentum $D(0)$ using the function $A + B/N^\nu$, where N is the lattice side in lattice units. This gives[12]

$$A = -0.002 \pm 0.010 \quad (64)$$

$$B = 1.7 \pm 0.8 \quad (65)$$

$$\nu = 0.7 \pm 0.1, \quad (66)$$

with $\chi^2/\mathrm{d.o.f.} = 1.07$ (considering seven data points). The fit improves if one sets $A = 0$. Indeed, in this case we find

$$B = 1.9 \pm 0.2 \quad (67)$$

$$\nu = 0.71 \pm 0.02 \quad (68)$$

with $\chi^2/\mathrm{d.o.f.} = 0.87$. Thus, the value of the parameter s in $f_7(p^2)$ [see Eq. (55)] is consistent with zero at infinite-volume, implying $D(0) = 0$ in the same limit. One should note, however, that the condition $D(0) = 0$ is not obtained here with $b = 0$ and $\upsilon = 0$ [see Eqs. (56) and (57)], i.e. with purely imaginary poles as in a Gribov-like propagator

[12]Recall that, with our notation, the $2d$ gluon propagator is dimensionless.

TABLE XII. Fits of the gluon-propagator data in the $2d$ case, for different lattice volumes, using the fitting function $f_7(p^2)$ in Eq. (55) and unimproved momenta [see Eq. (26)]. We report, besides the value of the fit parameters, the χ^2/d.o.f. obtained in each case. The whole range of momenta was considered for the fit. Errors shown in parentheses correspond to one standard deviation.

V	$C(\mathrm{GeV}^2)$	$u(\mathrm{GeV})$	$t(\mathrm{GeV}^2)$	$s(\mathrm{GeV}^2)$	$l(\mathrm{GeV}^{2-\eta})$	η	χ^2/d.o.f.
80^2	0.073 (0.005)	0.363 (0.041)	0.265 (0.011)	0.078 (0.008)	0.403 (0.142)	1.129 (0.151)	2.92
120^2	0.069 (0.004)	0.432 (0.027)	0.252 (0.008)	0.052 (0.005)	0.566 (0.128)	1.145 (0.088)	2.75
160^2	0.067 (0.004)	0.458 (0.022)	0.250 (0.007)	0.044 (0.003)	0.665 (0.117)	1.138 (0.066)	2.68
200^2	0.068 (0.003)	0.470 (0.022)	0.254 (0.007)	0.037 (0.003)	0.653 (0.104)	1.088 (0.057)	3.22
240^2	0.069 (0.002)	0.469 (0.018)	0.252 (0.005)	0.031 (0.002)	0.626 (0.076)	1.051 (0.041)	2.61
280^2	0.069 (0.002)	0.483 (0.016)	0.261 (0.005)	0.029 (0.002)	0.648 (0.064)	0.994 (0.033)	2.34
320^2	0.070 (0.002)	0.483 (0.016)	0.260 (0.005)	0.025 (0.002)	0.630 (0.062)	0.981 (0.032)	2.77

TABLE XIII. Fits of the gluon-propagator data in the $2d$ case, for different lattice volumes, using the fitting function $f_7(p^2)$ in Eq. (55) and improved momenta [see Eq. (27)]. We report, besides the value of the fit parameters, the χ^2/d.o.f. obtained in each case. The whole range of momenta was considered for the fit. Errors shown in parentheses correspond to one standard deviation.

V	$C(\mathrm{GeV}^2)$	$u(\mathrm{GeV})$	$t(\mathrm{GeV}^2)$	$s(\mathrm{GeV}^2)$	$l(\mathrm{GeV}^{2-\eta})$	η	χ^2/d.o.f.
80^2	0.114 (0.002)	0.433 (0.031)	0.207 (0.012)	0.031 (0.004)	0.026 (0.043)	0.684 (0.594)	2.63
120^2	0.112 (0.003)	0.486 (0.024)	0.197 (0.008)	0.020 (0.002)	0.091 (0.050)	1.003 (0.186)	2.51
160^2	0.110 (0.002)	0.503 (0.020)	0.199 (0.006)	0.018 (0.001)	0.133 (0.044)	1.027 (0.111)	2.31
200^2	0.110 (0.002)	0.523 (0.020)	0.201 (0.007)	0.015 (0.001)	0.157 (0.046)	1.017 (0.092)	2.92
240^2	0.110 (0.002)	0.519 (0.018)	0.201 (0.006)	0.013 (0.001)	0.152 (0.038)	0.955 (0.073)	3.06
280^2	0.110 (0.002)	0.530 (0.016)	0.208 (0.006)	0.012 (0.001)	0.168 (0.033)	0.904 (0.055)	2.77
320^2	0.110 (0.001)	0.539 (0.015)	0.209 (0.006)	0.011 (0.001)	0.180 (0.033)	0.909 (0.049)	2.91

(12), but it seems to be due to the relations $a = -b$ and $v = w$ (see Table XIV). Thus, the behavior in the $2d$ case appears closer to the RGZ propagator (18) (with a non-integer power in the numerator) than to a GZ propagator (12). However, as mentioned in the Introduction, one cannot relate the fitting parameters to dimension-two condensates in the $2d$ case.

Finally, taking into account the infinite-volume limit, we set $s = 0$ in $f_7(p^2)$. In this case, the gluon propagator at small momenta behaves as $D(p^2) \approx Clp^\eta/t^2$. From the conformal relation (see, for example, Ref. [57] with $d = 2$)

$$D(p^2) \sim (p^2)^{2\kappa+(4-d)/2-1} = p^{4\kappa} \tag{69}$$

we find the IR exponent $\kappa \approx 0.225$ using $\eta \approx 0.9$ (see Table XIII). This result is in reasonable agreement with the numerical estimate in Ref. [57].

VIII. CONCLUSIONS

We have performed a systematic fitting analysis of Landau-gauge gluon-propagator data for SU(2) gauge theory in 2, 3, and 4 space-time dimensions. The fit results were matched to analytic predictions from the RGZ framework, with the intent of calculating values in physical units for the dimension-two condensates in the theory, as well as to test the predictions in a neutral way. Indeed, as mentioned in the Introduction, our strategy has been firstly to find fits with convenient free parameters in simple (rational, except for $2d$) forms and then to interpret the parameters in terms of physical quantities. In that way, we do not bias the fits by imposing relations between fit parameters from the predicted forms. In particular, a direct fit to the general RGZ formula [see Eq. (17)] would involve six parameters (corresponding to the four condensates, the parameter λ^4 and the overall normalization) with prescribed relations among them. On the contrary, our best fits in the $4d$ and $3d$ cases involve, respectively, four and five free parameters (including the overall normalization), considering all generated data points.[13] We find that the resulting fits of the infrared gluon propagator in $3d$ and $4d$ agree remarkably well with the tree-level predictions from the RGZ scenario. Nonperturbative effects are, of course, encoded in the values obtained from the fits for the condensates and for the Gribov parameter γ.[14]

In particular, the $4d$ results are well described by the simplified version of the RGZ gluon propagator in Eq. (18), equivalent to the simplest Gribov-Stingl form. This corresponds to a pair of complex-conjugate poles, as opposed to the Gribov propagator, in which the poles would be purely imaginary. Our fit results—using improved momenta and the fitting function $f_1(p^2)$ in

[13]We recall, however, the importance of considering improved momenta [see Eq. (27)] for the fits.

[14]A continuum extrapolation of the numerical values obtained for these quantities is postponed to a future study.

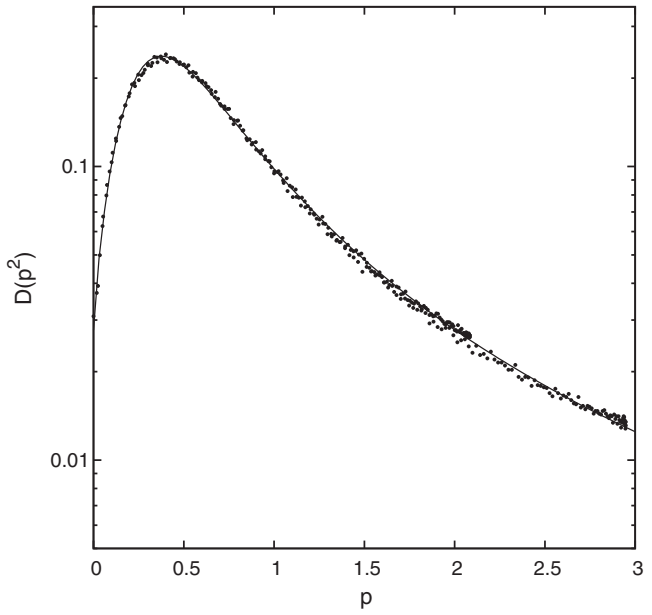

FIG. 5. Plot of the $2d$ gluon propagator $D(p^2)$ as a function of the (improved) momentum p (in GeV) for the lattice volume $V = 320^2$. We also show the fitting function $f_7(p^2)$ [see Eq. (55)] with the parameters reported in the last row of Table XIII. Note that in $2d$, with our convention, the gluon propagator $D(p^2)$ is dimensionless. Also note the logarithmic scale on the y axis.

Eq. (28)—are given in Table II. The condensates and pole masses obtained for the largest lattice size are given, respectively, in Tables III and IV. The values for the condensates $M^2 + \rho_1$, m^2 and λ^4 are in agreement with the ones obtained for the SU(3) case in Ref. [24], where the analysis was done using a slightly different notation, as previously explained. The quantitative agreement between the infrared limit of SU(2) and SU(3) theories was observed numerically before in [16,73].

In $3d$, our fits support the more general form of the RGZ propagator in Eq. (17). Fit results—using improved momenta and the fitting function $f_4(p^2)$ in Eq. (36)—are given in Table IX, while condensates and pole masses from the largest lattice size are reported in Tables X and XI. In this case, the condensate ρ is a complex quantity and there are significant differences in the values of the other condensates and of λ^4 compared to the $4d$ case. Also, in $3d$ one has a real pole mass in addition to the pair of complex-conjugate poles. It is interesting to note that the masses from the complex poles assume similar values in $3d$ and $4d$, with an imaginary part that is more than twice their real part. (We recall that a Gribov propagator would have a null real part.) Note also that the mass and the coefficient associated with the real pole in $3d$ are very small.

TABLE XIV. Estimates of the parameters of the function $f_8(p^2)$ [see Eq. (56)] from fits (see last row of Table XIII above) to the equivalent form $f_7(p^2)$ in Eq. (55). Errors are obtained using propagation of error, a Monte Carlo analysis with 10 000 samples and a bootstrap analysis with 500 samples. In all cases we considered the volume $V = 320^2$ and improved momenta. Errors shown in parentheses correspond to one standard deviation. Note that the value of η can be obtained from the last row of Table XIII for propagation of error and Monte Carlo analysis, and from Eq. (63), for the bootstrap analysis.

parameter	propagation of error	Monte Carlo analysis	bootstrap analysis
a (GeV^2)	0.0550 (5)	0.0550 (5)	0.0559 (7)
b (GeV^2)	−0.049(8)	−0.049(7)	−0.037(2)
c (GeV$^{2-\eta}$)	0.07 (1)	0.07 (1)	0.089 (8)
υ (GeV^2)	0.145 (8)	0.145 (8)	0.151 (7)
w (GeV^2)	0.15 (2)	0.15 (1)	0.205 (6)

In the $2d$ case, two particular features arise in the analysis of the data. First, as known from previous lattice studies, the description of the infrared behavior of the gluon propagator $D(p^2)$ requires a noninteger power η of the momentum p. [See the fitting form $f_7(p^2)$ in Eq. (55) and fit parameters obtained using improved momenta in Table XIII.] Second, the pole structure that best fits the data is similar to the one observed in the $3d$ and $4d$ cases—i.e. complex-conjugate poles with nonzero real part—at all considered (finite) lattice volumes. In the infinite-volume limit, one finds $D(0) = 0$, as would be the case for a Gribov propagator, with purely imaginary poles. However, in our case, the real part of the poles does not seem to vanish in this limit. The null value of $D(0)$ comes, instead, from an exact cancellation of the contributions from the two complex-conjugate poles (see values of pole masses in Table XIV).

Our analysis strongly suggests—in $d = 2, 3, 4$—a pole structure with complex-conjugate masses (with comparable real and imaginary parts) for the infrared gluon propagator in Landau gauge.[15] As stressed at the end of Sec. III, one can interpret this result as describing an unstable particle [3,36,37]. In particular, by considering the position $m_g^2 - i m_g \Gamma_g$ of the gluon pole, one can estimate the gluon mass m_g and its width Γ_g, which are in principle gauge-independent quantities [77,78]. In our case, if we take as a reference the pole masses in the $4d$ case—i.e. the values $\omega_{\pm}^2 = \upsilon \pm iw$ with $\upsilon \approx 0.3$ GeV^2 and $w \approx 0.65$ GeV^2 from Table IV—we obtain

$$m_g \approx 550 \text{ MeV} \quad \text{and} \quad \Gamma_g \approx 1180 \text{ MeV}. \tag{70}$$

Note that the value for the gluon mass m_g is in agreement with other determinations [24,29,79,80].[16] At the same

[15] Let us mention that this complex-conjugate pole structure has been shown to describe also the longitudinal and transverse gluon propagators in Landau gauge at finite temperature [74–76], at least up to twice the critical temperature T_c.

[16] Let us remark that in Ref. [81] the authors prefer to consider, instead of the gluon mass m_g, the maximum wavelength of (confined) gluons, roughly corresponding to the inverse gluon mass $1/m_g$.

time, the very large value for the width Γ_g would correspond to a lifetime τ_g smaller than 10^{-24} s, supporting the existence of very short-lived excitations of the gluon field.

In summary, we have presented fits—inspired by an analytic prediction, i.e. the tree-level RGZ expression, which is equivalent to the Stingl formulation (see discussion at the end of Sec. III)—allowing a good description of lattice data for the Landau-gauge SU(2) gluon propagator $D(p^2)$. The data points range from about 4 GeV down to 20–40 MeV, which are the smallest simulated momenta to date. Our results thus provide an accurate modeling of $D(p^2)$ in the whole IR region using a simple rational expression, whose parameters may be interpreted as (effective) values for the condensates in the RGZ theory. This parametrization will hopefully be a useful input in future studies of the IR sector of Yang-Mills theories.

ACKNOWLEDGMENTS

D. Dudal and N. Vandersickel are supported by the Research-Foundation Flanders (FWO). A. Cucchieri and T. Mendes thank CNPq and FAPESP for partial support. A. Cucchieri also acknowledges financial support from the Special Research Fund of Ghent University (BOF UGent).

[1] J. Greensite, Prog. Part. Nucl. Phys. **51**, 1 (2003).
[2] V. N. Gribov, Nucl. Phys. **B139**, 1 (1978).
[3] D. Zwanziger, Nucl. Phys. **B364**, 127 (1991).
[4] D. Dudal, J. A. Gracey, S. P. Sorella, N. Vandersickel, and H. Verschelde, Phys. Rev. D **78**, 065047 (2008).
[5] A. Cucchieri and T. Mendes, Proc. Sci., LAT2007 (2007) 297.
[6] A. Cucchieri and T. Mendes, Phys. Rev. Lett. **100**, 241601 (2008).
[7] A. Cucchieri and T. Mendes, Phys. Rev. D **78**, 094503 (2008).
[8] A. Cucchieri and T. Mendes, Proc. Sci., QCD-TNT09 (2009) 026.
[9] A. Cucchieri, D. Dudal, T. Mendes, and N. Vandersickel (unpublished).
[10] A. C. Aguilar, D. Binosi, and J. Papavassiliou, J. High Energy Phys. 01 (2012) 050.
[11] D. Zwanziger, Nucl. Phys. **B399**, 477 (1993).
[12] D. Zwanziger, Phys. Rev. Lett. **90**, 102001 (2003).
[13] D. Zwanziger, Nucl. Phys. **B323**, 513 (1989).
[14] D. Zwanziger, Nucl. Phys. **B412**, 657 (1994).
[15] I. L. Bogolubsky, E. M. Ilgenfritz, M. Muller-Preussker, and A. Sternbeck, Proc. Sci., LAT2007 (2007) 290.
[16] A. Sternbeck, L. von Smekal, D. B. Leinweber, and A. G. Williams, Proc. Sci., LAT2007 (2007) 340.
[17] I. L. Bogolubsky, E. M. Ilgenfritz, M. Muller-Preussker, and A. Sternbeck, Phys. Lett. B **676**, 69 (2009).
[18] V. G. Bornyakov, V. K. Mitrjushkin, and M. Muller-Preussker, Phys. Rev. D **81**, 054503 (2010).
[19] A. Cucchieri, T. Mendes, and A. R. Taurines, Phys. Rev. D **71**, 051902 (2005).
[20] A. C. Aguilar, D. Binosi, and J. Papavassiliou, Phys. Rev. D **78**, 025010 (2008).
[21] C. S. Fischer, A. Maas, and J. M. Pawlowski, Ann. Phys. (N.Y.) **324**, 2408 (2009).
[22] D. Binosi and J. Papavassiliou, Phys. Rep. **479**, 1 (2009).
[23] T. Iritani, H. Suganuma, and H. Iida, Phys. Rev. D **80**, 114505 (2009).
[24] D. Dudal, O. Oliveira, and N. Vandersickel, Phys. Rev. D **81**, 074505 (2010).
[25] A. C. Aguilar, D. Binosi, and J. Papavassiliou, J. High Energy Phys. 07 (2010) 002.
[26] A. Cucchieri, T. Mendes, Phys. Rev. D **81**, 016005 (2010).
[27] M. Tissier and N. Wschebor, Phys. Rev. D **82**, 101701 (2010).
[28] M. R. Pennington and D. J. Wilson, Phys. Rev. D **84**, 119901 (2011).
[29] O. Oliveira and P. Bicudo, J. Phys. G **38**, 045003 (2011).
[30] A. C. Aguilar, D. Binosi, and J. Papavassiliou, Phys. Rev. D **81**, 125025 (2010).
[31] M. Tissier and N. Wschebor, Phys. Rev. D **84**, 045018 (2011).
[32] H. Aiso *et al.*, Nucl. Phys. B, Proc. Suppl. **53**, 570 (1997).
[33] D. B. Leinweber, J. I. Skullerud, A. G. Williams, and C. Parrinello (UKQCD Collaboration), Phys. Rev. D **60**, 094507 (1999); **60**, 094507 (1999).
[34] J. E. Mandula, Phys. Rep. **315**, 273 (1999).
[35] A. Cucchieri, T. Mendes, and A. R. Taurines, Phys. Rev. D **67**, 091502 (2003).
[36] M. Stingl, Phys. Rev. D **34**, 3863 (1986); **36**, 651(E) (1987).
[37] M. Stingl, Z. Phys. A **353**, 423 (1996).
[38] D. Dudal, J. A. Gracey, S. P. Sorella, N. Vandersickel, and H. Verschelde, Phys. Rev. D **78**, 125012 (2008).
[39] N. Vandersickel, D. Dudal, and S. P. Sorella, Proc. Sci., FACESQCD (2010) 044.
[40] N. Vandersickel, arXiv:1104.1315.
[41] D. Dudal, S. P. Sorella, and N. Vandersickel, Phys. Rev. D **84**, 065039 (2011).
[42] D. Dudal, S. P. Sorella, N. Vandersickel, and H. Verschelde, Phys. Lett. B **680**, 377 (2009).
[43] N. Maggiore and M. Schaden, Phys. Rev. D **50**, 6616 (1994).
[44] D. Dudal, S. P. Sorella, and N. Vandersickel, Eur. Phys. J. C **68**, 283 (2010).
[45] R. F. Sobreiro, S. P. Sorella, D. Dudal, and H. Verschelde, Phys. Lett. B **590**, 265 (2004).
[46] D. Zwanziger, Phys. Lett. B **257**, 168 (1991).
[47] J. A. Gracey, Braz. J. Phys. **37**, 226 (2007).
[48] F. R. Ford and J. A. Gracey, J. Phys. A **42**, 325402 (2009).
[49] D. Zwanziger, Phys. Rev. D **81**, 125027 (2010).
[50] Y. L. Dokshitzer and D. E. Kharzeev, Annu. Rev. Nucl. Part. Sci. **54**, 487 (2004).

[51] R. Alkofer, W. Detmold, C. S. Fischer, and P. Maris, Phys. Rev. D **70**, 014014 (2004).
[52] C. W. Bernard, C. Parrinello, and A. Soni, Nucl. Phys. B, Proc. Suppl. **30**, 535 (1993).
[53] A. Cucchieri and T. Mendes, Phys. Rev. D **73**, 071502 (2006).
[54] http://www.usp.br/lcca/IBM.html.
[55] A. Cucchieri and T. Mendes, Nucl. Phys. **B471**, 263 (1996).
[56] J. C. R. Bloch, A. Cucchieri, K. Langfeld, and T. Mendes, Nucl. Phys. **B687**, 76 (2004).
[57] A. Maas, Phys. Rev. D **75**, 116004 (2007).
[58] A. Cucchieri, Nucl. Phys. **B508**, 353 (1997).
[59] P. J. Silva and O. Oliveira, Nucl. Phys. **B690**, 177 (2004).
[60] I. L. Bogolubsky, G. Burgio, M. Muller-Preussker, and V. K. Mitrjushkin, Phys. Rev. D **74**, 034503 (2006).
[61] I. L. Bogolubsky, E. M. Ilgenfritz, M. Muller-Preussker, and A. Sternbeck, Proc. Sci., LATTICE2009 (2009) 237.
[62] A. Maas, J. M. Pawlowski, D. Spielmann, A. Sternbeck, and L. von Smekal, Eur. Phys. J. C **68**, 183 (2010).
[63] S. Furui and H. Nakajima, Few-Body Syst. **40**, 101 (2006).
[64] E. M. Ilgenfritz, M. Muller-Preussker, A. Sternbeck, A. Schiller, and I. L. Bogolubsky, Braz. J. Phys. **37**, 193 (2007).
[65] P. O. Bowman *et al.*, Phys. Rev. D **76**, 094505 (2007).
[66] P. Boucaud *et al.*, Nucl. Phys. B, Proc. Suppl. **106**, 266 (2002).
[67] A. Cucchieri, T. Mendes, G. Travieso, and A. R. Taurines, *15th Symposium on Computer Architecture and High Performance Computing (SBAC-PAD'03)* (2003), p. 123.
[68] A. Cucchieri, Phys. Rev. D **60**, 034508 (1999).
[69] J. P. Ma, Mod. Phys. Lett. A **15**, 229 (2000).
[70] F. de Soto and C. Roiesnel, J. High Energy Phys. 09 (2007) 007.
[71] http://www.gnuplot.info/documentation.html.
[72] A. Cucchieri and T. Mendes, AIP Conf. Proc. **1343**, 185 (2011).
[73] A. Cucchieri, T. Mendes, O. Oliveira, and P. J. Silva, Phys. Rev. D **76**, 114507 (2007).
[74] A. Cucchieri and T. Mendes, Proc. Sci., LATTICE2010 (2010) 280.
[75] A. Cucchieri and T. Mendes, Proc. Sci., FACESQCD (2010) 007.
[76] A. Cucchieri and T. Mendes (unpublished).
[77] N. K. Nielsen, Nucl. Phys. **B101**, 173 (1975).
[78] P. A. Grassi, B. A. Kniehl, and A. Sirlin, Phys. Rev. D **65**, 085001 (2002).
[79] A. A. Natale, Braz. J. Phys. **37**, 306 (2007).
[80] P. Boucaud *et al.*, Phys. Rev. D **82**, 054007 (2010).
[81] S. J. Brodsky and R. Shrock, Phys. Lett. B **666**, 95 (2008).